NIH Public Access
Author Manuscript
Neuron. Author manuscript; available in PMC 2010 October 29.

Published in final edited form as:
Neuron. 2009 October 29; 64(2): 200–212. doi:10.1016/j.neuron.2009.09.021.

Spatial-Temporal Patterns of Retinal Waves Underlying Activity-Dependent Refinement of Retinofugal Projections

Ben K. Stafford[1], **Alexander Sher**[2,3], **Alan M. Litke**[2,*], and **David A. Feldheim**[1,*]

[1] Department of Molecular, Cell, and Developmental Biology, University of California, Santa Cruz, Santa Cruz, Ca. 95064

[2] Santa Cruz Institute of Particle Physics, University of California, Santa Cruz, Santa Cruz, Ca. 95064

[3] Department of Physics, University of California, Santa Cruz, Santa Cruz, Ca. 95064

Abstract

During development, retinal axons project coarsely within their central visual targets before refining to form precisely organized synaptic connections. Spontaneous retinal activity, in the form of acetylcholine-driven retinal waves, is widely proposed to be necessary for establishing these precise projection patterns. In particular, both axonal terminations of retinal ganglion cells (RGCs) and the size of receptive fields of neurons in visual areas of the brain are larger in mice that lack the β2 subunit of the nicotinic acetylcholine receptor (β2KO). Here, using a large-scale, high-density multi-electrode array to record single-unit activity from hundreds of RGCs simultaneously, we present analysis of early post-natal retinal activity from both wild type (WT) and β2KO retinas. We find that β2KO retinas have correlated patterns of activity, but many aspects of these patterns differ from those of WT retina. Quantitative analysis of these differences suggests that wave directionality, coupled with short-distance correlated bursting patterns of RGCs, work together to drive refinement of retinofugal projections.

Introduction

The development of the central nervous system (CNS) depends upon the formation of precise neuronal connections. To establish this connectivity, developing axons use a combination of molecular cues that guide them to their approximate position in their target as well as activity-dependent mechanisms that refine their connections through a combination of synaptic strengthening and elimination (Huberman et al., 2008). Two well-studied examples of such precise connectivity are topographic mapping and eye-specific segregation in the visual system. In the mammalian visual system, retinal ganglion cells (RGCs) from each eye send projections to multiple targets on both sides of the brain. Two primary targets are the dorsal lateral geniculate nucleus (dLGN) in the thalamus, and the superior colliculus (SC) in the midbrain. In each area, RGC axons form a continuous topographic map whereby the spatial relationships of projecting neurons are maintained in the target. Within the dLGN, inputs from the two eyes segregate such that projections from each eye form two non-overlapping eye-specific domains.

*Correspondence: feldheim@biology.ucsc.edu; Alan.Litke@cern.ch.

Publisher's Disclaimer: This is a PDF file of an unedited manuscript that has been accepted for publication. As a service to our customers we are providing this early version of the manuscript. The manuscript will undergo copyediting, typesetting, and review of the resulting proof before it is published in its final citable form. Please note that during the production process errors may be discovered which could affect the content, and all legal disclaimers that apply to the journal pertain.

NIH-PA Author Manuscript
NIH-PA Author Manuscript
NIH-PA Author Manuscript

NIH-PA Author Manuscript

NIH-PA Author Manuscript

NIH-PA Author Manuscript

In the mouse, retinocollicular and retinogeniculate projections undergo rapid remodeling during the first two weeks of life (Godement et al., 1984; So et al., 1990; Simon and O'Leary, 1992). At birth, axons project diffusely within their targets before establishing rough topography in the SC and overlapping eye-specific domains in the dLGN by the middle of the first post-natal week. Over the next week, these coarse projections refine to form adult-like projection patterns. During this time, RGCs discharge highly correlated bursts of activity that propagate across the retina as waves that have been theorized to drive refinement through activity-dependent mechanisms (Meister et al., 1991; Wong et al., 1993; Butts and Rokhsar, 2001; Butts et al., 2007). Perhaps the most compelling evidence that activity-dependent processes regulate refinement of the visual pathway came from studies of mice lacking the β2 subunit (β2KO) of the nicotinic acetylcholine receptor (nAch) (Picciotto et al., 1995; Xu et al., 1999). Retinal waves during the first post-natal week of life require cholinergic neurotransmission, and β2KO retinas have been reported to lack acetylcholine-mediated waves during this time (Feller et al., 1996; Bansal et al., 2000; McLaughlin et al., 2003). In these mice, both retintopy and eye-specific segregation fail to develop normally (Muir-Robinson et al., 2002; Grubb et al., 2003; McLaughlin et al., 2003; Chandrasekaran et al., 2005; Mrsic-Flogel et al., 2005; Chandrasekaran et al., 2007).

Despite these data from β2KO mice supporting a crucial role for retinal waves in activity-dependent refinement of the visual system, it is unclear which aspects of spontaneous retinal activity are important for driving activity-dependent refinement (Chalupa, 2007). Further, a recent paper showing that β2KO retinas can produce retinal waves in vitros suggests that the β2KO mouse may not be suitable for assessing the role of correlated activity in visual system development (Sun et al., 2008). While these results indicate that the refinement defects in β2KO mice cannot be attributed to a complete absence of retinal waves, understanding whether there are changes in specific aspects of retinal waves that could account for these defects is critical for understanding the mechanisms of activity-dependent refinement in the CNS.

In this study, we re-examine the spatial-temporal properties of spontaneous retinal activity in early post-natal retinas isolated from wild type (WT) and β2KO mice using a large-scale, high-density MEA (Litke et al., 2004). Recordings using this MEA detect single-unit responses from hundreds of RGCs in a single preparation encompassing nearly half of an early post-natal retina and allows us to evaluate aspects of retinal waves not possible using other methods. We find that the patterns of activity in β2KO, but not WT retina, are temperature dependent, such that β2KO retinas produce retinal waves only at higher temperatures (37°C). We also find that the dynamics of retinal waves and the discharge properties of RGCs differ in several key aspects between β2KO and WT retinas. We find that WT, but not β2KO, waves travel with a directional bias. We also find that, during waves, RGCs in β2KO retinas fire bursts that are correlated over longer distances than in WT retinas and that β2KO RGCs spend less time firing high-frequency bursts than do WT RGCs. Finally, we demonstrate that the majority of RGC bursts are not associated with retinal waves in β2KO retinas and, therefore, are not significantly correlated with one another. Taken together these data suggest that the directional preference of waves, combined with precisely correlated, high-frequency bursting of individual RGCs, encodes the information used to refine visual system connections.

Results

To better understand the physiological properties of retinal waves and determine which of these properties are disrupted in the β2KO mouse, we characterized the spontaneous retinal activity patterns in WT and β2KO retinas using a large-scale MEA. This MEA contains 512 electrodes in a 32 × 16 rectangular pattern with an interelectrode spacing of 60 μm, yielding a recording area of 1.7 mm^2, and allows us to record from approximately half of an early post-natal mouse retina (Litke et al., 2004). In a typical two hour recording, we isolate single-unit responses from

NIH-PA Author Manuscript

NIH-PA Author Manuscript

NIH-PA Author Manuscript

several hundred RGCs simultaneously. This represents a roughly 5-fold improvement over reports using MEAs containing 61 electrodes and allows us to detect unique properties of retinal waves (Table S1). Because previous work employed a range of temperatures with differing results, we performed recordings at both 30°C and 37°C and in some cases recorded from a retinal preparation for 1 hour at 30°C before shifting to 37°C. Using custom written software, we used principal components analysis followed by an expectation maximization clustering algorithm to isolate signals from individual RGCs and analyzed multiple aspects of spontaneous activity patterns (Litke et al., 2004).

Temperature dependent wave formation in β2KO retina

Recordings from P6 WT mouse retinas confirmed previous results (Demas et al., 2003; McLaughlin et al., 2003; Stacy et al., 2005; Torborg et al., 2005; Demas et al., 2006; Sun et al., 2008) showing that RGCs produce spontaneous, correlated bursts of activity that propagate across the retina in the form of retinal waves at both 30°C and 37°C (Figures 1A, 2A; Movies S1, S2). Although the general characteristics of WT activity are similar at both temperatures, the propagation speed and frequency of waves as well as the mean spike rate increased when the temperature was increased to 37°C (Figures 1C, 2D, 2E). Hebbian models used to explain how RGC axons refine predict that an important function of retinal waves is to correlate the firing patterns of nearby RGC pairs and/or decorrelate firing patterns of distant RGC pairs (Torborg and Feller, 2005). To assess the degree of correlation we measured the correlation index (CI) between spikes from RGC pairs as a function of the distance between them (Meister et al., 1991; Wong et al., 1993). In WT retinas the probability of two RGCs firing together, defined as coincident spiking within a 100 millisecond coincidence interval, is extremely high within the first 250 μm, before declining to chance alone by ~600 μm, with only a slight shift in the overall correlation level depending on the temperature of the recording (Figure 1E, S1A).

Recordings from β2KO retinas revealed strikingly different patterns of spontaneous activity depending on the recording temperature. At 30°C, β2KO retinas did not produce retinal waves, although individual RGCs still produced asynchronous bursts of activity (Figure 1B, 2B; Movie S3). However, when the recording temperature was raised to 37°C, RGCs produced periodic synchronous bursts of activity that propagated across the retina as waves (Figure 1B, 2B; Movie S4). These waves were reliably produced when the temperature in the recording chamber reached 35-36°C and dissipated when retinas were shifted back to 30°C (data not shown). We also found that β2KO waves are larger and propagate faster than those in WT retinas (Figure 1C, 1D). Similar to WT, recording at 37°C increased the mean spike rate of the preparation, although the mean spike rate was not significantly different between WT and β2KO at either temperature (Figure 2D). The faster and larger waves lead to significant differences in the correlated firing patterns of β2KO retinas when compared to those of WT. In β2KO recordings at 37°C, the CI for RGC pairs separated by less than 300 μm is lower than WT, while the CI for pairs of RGCs separated by more than 300 μm is higher than WT (Figure 1E; S1A). These data suggest that the defects in mapping seen in β2KO mice are due to the altered patterns of activity we observe in β2KO at 37°C rather than a simple absence of retinal waves.

Directional bias of retinal waves is disrupted in β2KO retinas

One unexplained aspect of the mapping defects in β2KO mice is that, although both axes fail to refine normally, the refinement of fine-scale topography is 3-5 times weaker along the NT visual axis than along the dorsal-ventral (DV) axis (Grubb et al., 2003; Cang et al., 2005; Chandrasekaran et al., 2005). This implies that spontaneous activity may have an underlying structure that affects the NT axis more than the DV axis, which could arise if retinal waves travel preferentially along one axis. Previous reports using calcium imaging and either low density or small area MEAs failed to find a directional bias in retinal waves (Meister et al., 1991; Wong et al., 1993; Feller et al., 1997). However, given the finer spatial resolution, and

NIH-PA Author Manuscript

NIH-PA Author Manuscript

NIH-PA Author Manuscript

increased size of our MEA, we re-examined the directional bias of waves in WT and β2KO retinas.

To determine if there is a preferred wave direction in the developing retina, we recorded spontaneous activity from P6 WT and β2KO retinas from nasal, temporal, dorsal, and ventral retina where the orientation of the retina relative to the electrodes was known. We then assayed whether activity travels through individual RGCs with a directional bias by analyzing bursts fired by RGCs during waves. We calculated the directional bias vector of each RGC where the magnitude of the vector represents the strength of the directional bias, and the angle defines the angle of the bias of the RGC (see Methods). Using this calculation, we found that most RGCs show a directional bias (WT: 98%; β2KO: 86%) that is independent of quadrant (Between quadrants ANOVA: WT: $p = 0.9262$; β2KO: $p = 0.5751$) or genotype ($p = 0.1522$, ANOVA) indicating that, on average, waves travel through single RGCs in a stereotypical direction (Figure 3A, S1B; see Methods). We next calculated the directional bias vector of the preparation, which is the normalized vector sum of the directional bias of all the RGCs in a given preparation, and indicates whether waves travel in a preferred direction in a given preparation (see Methods). We found that waves in WT preparations have a directional bias and that the magnitude of this bias is similar in each retinal quadrant (WT: $p = 0.5427$, ANOVA; Figure 3B, C, E, S2). We also found that the angle of this directional bias varies depending upon retinal location. In dorsal, ventral, and temporal retina, the preferred direction of waves was from temporal-ventral to nasal-dorsal, while in nasal retina waves traveled more often in the opposite direction (Table 2). In β2KO preparations, we observed significantly smaller preparation directional bias in all retinal quadrants compared to that of the WT retinas (Figure 3B, S3). Furthermore, we found no systematic preparation directional bias between retinal quadrants in β2KO (Figure 3D, 3F), but did find a significant difference between the angle of directional bias in WT and β2KO in each of the four quadrants ($p < 0.001$ for each quadrant; Watson Test).

The directional bias of retinal waves suggests that RGCs located along the propagation axis of a given wave will have spatio-temporal correlation patterns that are different from RGCs located perpendicular to this axis. Along both axes, RGCs that are close together will fire bursts that overlap in time which might cause them to strengthen inputs onto common targets in the brain. Along the axis of wave propagation, RGCs separated by larger distances will be more likely to fire bursts that are temporally offset than RGCs located perpendicular to this axis. Temporally offset bursts have been proposed to weaken synapses and an axis-specific difference in the temporally offset bursting of RGCs could lead to an anisotropy at the level of topographic refinement of their projections (Dan and Poo, 2006; Butts et al., 2007). To determine the relevant temporal offset, we separated RGC pairs into two groups: those that lay along the axis of the preferred wave direction within a preparation and those that lay orthogonal to it. We then calculated the correlation index of bursts offset by differing time windows (offset correlation index, OCI) in each group and plotted the OCI versus distance between RGCs (Figure S6). We found that a time offset of between 4 and 5 seconds produces the greatest difference in OCI between the two axes and that this drives temporally offset bursts in RGCs separated by 800-1000 μm (Figure 4A). This difference was not seen in β2KO retinas, due to the lack of direction preference of waves in these retinas (Figure 4B). These data provide evidence that the directional bias of waves can produce axis-specific effects on spontaneous activity patterns and may provide an explanation for the greater influence of β2-dependent activity patterns on the mapping of the NT axis.

Physiological output of RGCs is altered in β2KOs

Computational and experimental work aimed at understanding the properties of retinal waves that are important for refinement suggest that bursts of action potentials are the unit of

NIH-PA Author Manuscript

NIH-PA Author Manuscript

NIH-PA Author Manuscript

information that is used to drive refinement (Butts and Rokhsar, 2001; Butts et al., 2007). Bursts with more spikes are theorized to transfer more information to the target, and there is evidence that bursts containing more spikes help drive activity-dependent refinement (Butts and Rokhsar, 2001; Torborg et al., 2005; Bjartmar et al., 2006; Demas et al., 2006). We hypothesized that differences in the spiking properties of bursts during waves between β2KO and WT RGCs could be responsible for the defects seen in the refinement of RGC projections in β2KO. We found that a significantly smaller percentage of spikes are included in bursts in β2KO retinas, reflecting the more tonic character of β2KO spike trains (Figure 5A). We also found that the inter-spike interval (ISI) of bursts is increased in β2KO RGCs, while the burst duration is unchanged (Figure 5B, C). These results are consistent with the idea that the bursts fired by β2KO RGCs contain fewer spikes and may transmit less information to target neurons.

RGC bursts are typically tightly associated with waves and this synchrony is thought to help mediate activity-dependent refinement (Meister et al., 1991; Wong et al., 1993; Feller et al., 1996; Torborg and Feller, 2005). This tight synchronization with waves is altered in β2KO retinas and to quantify the degree to which this synchronization is perturbed, we calculated the percent of all bursts that occurred during waves. We found that in WT retinas, nearly 90% of RGC bursts occur during waves (Figure 5D). In contrast, less than 40% of RGC bursts occur during waves in β2KO, even though burst frequency is increased compared to WT (Figure 5D; Table 1).

During waves, RGCs produce bursts with high spike rates, and periods of spiking above 10 Hz have been implicated in activity-dependent refinement (Torborg et al., 2005; Bjartmar et al., 2006; Demas et al., 2006). Therefore, we also analyzed high-frequency spiking, which we defined as periods of spiking above 10 Hz that occur during a burst. We found that WT RGCs spend more time spiking at high frequencies than β2KO RGCs (Table 1). Taken together, these data indicate that the majority of bursts fired by β2KO RGCs do not occur during waves and spend less time spiking at high frequencies.

We also tested whether the spiking properties of bursts fired by β2KO RGCs differed depending on whether they were part of a wave or not. To address this, we compared various spiking properties of RGCs during wave-bursts and non-wave-bursts. We found that the ISIs of bursts were not significantly different between wave-bursts and non-wave-bursts for both β2KO and WT (Table S2). We also found that WT RGCs spend more time spiking at high frequencies during wave-bursts than non-wave-bursts. In contrast, in β2KO retinas, RGCs spend more time spiking at high frequencies in non-wave-bursts (Figure 5E). Finally, we found that wave-bursts from pairs of RGCs separated by more than 100 μm are significantly more correlated in β2KO retinas than WT, while non-wave-bursts from pairs of β2KO RGCs are less correlated than WT wave-bursts at near distances and β2KO wave-bursts at all distances. (Figure 5F). Taken together, these data are consistent with the idea that, despite the presence of retinal waves, the majority of the bursts produced by β2KO RGCs contain less high-frequency spiking that is correlated and, therefore, is less likely to drive refinement.

Discussion

As is the case for many projections in the CNS, the projections from the retina to the SC and the dLGN initially project coarsely within their target regions, before refining to form precise connections. Refinement happens before eye-opening and requires cholinergic retinal waves as mice lacking the β2 subunit of the nAch receptor lack normal patterns of retinal waves and have defects in refinement (Feller et al., 1996; Grubb et al., 2003; McLaughlin et al., 2003; Cang et al., 2005). What is not known is how the information encoded by retinal waves drives this refinement. Here, using large-scale, high-density MEA recordings, we provide a comprehensive analysis of retinal waves in WT and β2KO mice. We show that retinas from

NIH-PA Author Manuscript

NIH-PA Author Manuscript

NIH-PA Author Manuscript

β2KO mice produce retinal waves in vitro at 37°C, but not at 30°C, while WT retinas produce waves at both temperatures. We also find that retinal waves travel with a NT bias in WT retinas and that this bias is absent in β2KOs. Finally, we show that the physiological output of RGCs is severely altered in β2KOs where bursts are uncorrelated and produce fewer high-frequency spikes. Taking into account the refinement defects present in these mice, our findings suggest that the directional bias of waves, coupled with precisely correlated bursting patterns play an important role in the refinement of retinofugal projections.

Retinal waves are present in β2KO

Previous reports showing that retinas derived from β2KO mice lacked retinal waves supported the hypothesis that they play an instructive role in eye-specific segregation and the formation of fine scale topography. These conclusions have been called into question by Sun et al. (2008) who showed that β2KO retinas produce retinal waves in vitro that can be disrupted by gap junction blockers (Sun et al., 2008). Here, we confirm these results and show that retinal waves are only present in β2KO retinas at higher temperatures; retinal waves rapidly emerge when the same retinal preparation is shifted from 30°C to 37°C (Figure 1B, 2B). Although the precise cause for the emergence of this correlated activity at higher temperatures is unknown, we hypothesize that retinal gap junction conductance may be temperature dependent as has been observed in gap junctions in other contexts (Chen and DeHaan, 1993; Valiunas et al., 1999). In addition, this finding is consistent with reports that retinal waves can be induced in β2KO retinas through non-synaptic mechanisms (Singer et al., 2001). Finally, mouse pups have been shown to maintain a body temperature of >35°C when isolated from their mothers for up to 15 minutes during the first post-natal week, and mothers spend approximately 90% of their time in contact with their litter (Pauluhn and Schmuck, 2003; Champagne et al., 2007). Thus it is most likely that the developing retina is maintained at temperatures that can promote waves in vitro.

Wave directionality helps refine the NT mapping axis

One unexplained aspect of the mapping defects in β2KO mice is that, although refinement of fine-scale topography is affected along both the NT and DV axes, these defects are larger along the NT axis. Axis-specific effects have been reported in the SC as preferential enlargement of receptive fields (RFs) along the NT axis, in the dLGN as blurring of fine-scale topography along the NT axis, and in the visual cortex where receptive field organization is disrupted along the NT axis (Grubb et al., 2003; Cang et al., 2005; Chandrasekaran et al., 2005; Mrsic-Flogel et al., 2005; Chandrasekaran et al., 2007). Our observation that retinal waves travel more frequently along the NT axis may provide an explanation for this.

The fact that retinal waves travel with a NT directional bias suggests that waves could influence this axis differently than the DV axis. Previous work has shown that when the start of a post-synaptic burst follows the end of a pre-synaptic burst by 1-2 seconds, synaptic weakening can be induced in retinogeniculate synapses (Butts et al., 2007). We find that anisotropic wave propagation causes RGCs separated by 800-1000 μm along the NT axis to have an increased probability of firing bursts that are offset in time when compared to RGCs located along the DV axis in WT but not β2KO mice (Figure 4, S6). Our data, therefore, suggest that the directional bias of waves could enhance synaptic weakening along the NT axis.

The use of retinal waves to weaken synapses preferentially along the NT mapping axis correlates well with what is known about the development of topographic map formation in the SC. At birth, RGC axons overshoot their targets by a millimeter or more along the NT mapping axis, but enter more topographically organized and overshoot much less along the DV mapping axis (Simon and O'Leary, 1992; Plas et al., 2005). A process that specifically weakens synapses from RGCs separated by 800-1000 μm along the NT axis of the retina will,

NIH-PA Author Manuscript

NIH-PA Author Manuscript

NIH-PA Author Manuscript

therefore, aid in correcting this early bias in the level of refinement between the two axes. Our data support a model where the directional bias of retinal waves serves to enhance the likelihood that spatially distant RGCs will fire temporally-offset bursts along the NT axis which helps drive refinement more effectively along this axis through the elimination of incorrect synapses (Figure 6A).

Previous reports that used calcium imaging or low density or small area MEAs in both mouse and ferret failed to find a directional bias in retinal waves (Meister et al., 1991; Wong et al., 1993; Feller et al., 1997). Our success is likely due to our ability to (1) record from a larger area of the retina; (2) record a larger number of waves for analysis; and (3) record from a more locally complete population of neurons. When we sub-sample our data either by analyzing just the first 20 minutes of our recordings or by utilizing a 60 electrode configuration, we fail to find a reproducible directional bias (Figure S4).

It is also interesting to note that the directional bias of retinal waves does not fall on the true NT axis of the retina, but instead is shifted ~35° clockwise (Figure 3C; Table 2). At this time we don't know whether such a shift might contribute to activity-dependent mapping, but it is of interest given that others have reported shifts of a similar magnitude of both the NT and DV axes in the SC (Drager and Hubel, 1976). Thus, it is tempting to speculate that the directional bias of retinal waves might help establish these shifted mapping axes in the SC.

Specific bursting defects can account for the β2KO mapping defects

Spontaneous retinal activity has been hypothesized to drive two different aspects of refinement in distinct ways (Torborg and Feller, 2005). First, it helps drive fine-scale refinement by correlating the activity of nearby RGCs in time. Second, it assists in eye-specific segregation in the dLGN by ensuring that inputs from both eyes are unlikely to be active at the same time. The previously reported absence of retinal waves during the first post-natal week in β2KO mice, coupled with the refinement defects in these mice, has been taken as compelling evidence that correlated spontaneous activity plays a role in both of these processes. However, our recordings demonstrate that β2KO retinas produce waves in vitro at 37°C and our analyses indicate that the level of correlation amongst both spikes and bursts decreases as a function of distance in β2KO retinas (Figures 1 and 4). Therefore, something other than a complete absence of correlated activity must account for the mapping errors present in β2KO mice. Furthermore, although the mapping defects present in β2KO mice are enhanced along the NT axis, mapping of the DV axis is also perturbed, indicating that the loss directionally-biased retinal waves cannot account for all of the mapping errors in these mice (Cang et al., 2005; Chandrasekaran et al., 2005; Chandrasekaran et al., 2007). What then can account for these remaining defects?

One possible explanation comes from our observation that RGC bursts during waves in β2KO retinas are correlated over longer distances than those in the WT retina (Figure 5). We found that correlations are dramatically enhanced between RGCs separated by 200-600 μm. If fine-scale topography forms through a Hebbian-like mechanism, the stronger correlations between more distant neurons may cause them to be active at the same time and fail to refine properly (Katz and Shatz, 1996;Torborg and Feller, 2005). Based upon the mapping of the visual field onto the retina in mice, the retinal diameter of collicular RFs expand from 150-200 μm in WT to 400-600 μm in β2KO (Remtulla and Hallett, 1985;Schmucker and Schaeffel, 2004;Chandrasekaran et al., 2005). Our findings are consistent with this increase and suggest that this defect could help block refinement at this scale.

A second possibility for why RGC axons fail to refine in β2KO mice may be because RGCs fire bursts that contain fewer spikes, and therefore longer ISIs, and the bulk of their high-frequency spiking is uncorrelated (Figure 5). Synaptic remodeling at retinogeniculate and visual cortical synapses has been shown to be sensitive to both the ability of pre-synaptic bursts

NIH-PA Author Manuscript

NIH-PA Author Manuscript

NIH-PA Author Manuscript

to drive post-synaptic spiking and the timing of this coincident activity (Shatz and Stryker, 1988;Sjöström et al., 2001;Butts et al., 2007). Thus, the ability of bursts to elicit post-synaptic spiking is likely to play a role in driving fine-scale refinement of RGC projections. Bursts with shorter ISIs are more effective at inducing post-synaptic spiking in retinogeniculate synapses (Usrey et al., 1998;Chen and Regehr, 2000). Therefore, our findings that β2KO RGCs fire bursts with longer ISIs and altered spatial correlations are consistent with the idea that β2KO RGCs overwhelm target neurons with weak, poorly-correlated activity. This fails to induce proper post-synaptic spiking and refinement fails to occur (Figure 6B).

In addition to the lack of fine-scale topography in β2KO mice, retinogeniculate inputs fail to segregate properly in the dLGN. As outlined above, axonal projections are thought to segregate in the dLGN because inter-wave intervals (IWIs) decrease the likelihood that inputs from retinotopically matched positions in the two eyes will fire simultaneously (Torborg and Feller, 2005; Huberman, 2007). Manipulations that alter this likelihood, for example by increasing wave frequency, disrupt segregation (Stellwagen and Shatz, 2002; Demas et al., 2006). In β2KO retinas, we found that over half of the bursts occur between waves, indicating that retinal activity lacks well-defined IWIs (Figure 5). This should increase the probability that activity from the two eyes will be coincident in the target and, therefore, will fail to drive segregation. Our findings also help explain reports that intraocular injections of the cholinergic agonist epibatidine disrupt eye-segregation in vivo (Penn et al., 1998; Chandrasekaran et al., 2005; Pfeiffenberger et al., 2005), a treatment recently shown to increase the amount of activity in half of the RGCs while silencing the remainder (Sun et al., 2008). In light of our analysis of RGC firing patterns in β2KO mice, the increased activity in half of the RGCs in epibatidine treated mice likely increases the probability that the two eyes will fire simultaneously in the target. Thus, we favor a model whereby eye-specific segregation is disrupted in β2KO mice because inputs from each eye are more likely to fire at the same time despite the presence of retinal waves (Figure 6C).

It is also important to note that the majority of the differences in RGC spiking properties that we report here are consistent with those reported by Sun et al. (2008) with two exceptions (Sun et al., 2008). First, we found that wave frequency is increased while Sun et al. (2008) reported a decrease. This could be due to the fact that we defined waves mathematically while Sun et al. (2008) selected waves manually (Legendy and Salcman, 1985; Stacy et al., 2005). Second, we found no difference in the mean spike rate of WT and β2KO neurons while Sun et al. (2008) reported a dramatic increase in the spike rate of β2KO retinas. This difference might be attributed to the fact that they performed their recordings in MEM, a media that they demonstrated increases spike rates only in β2KO retinas, while ours were conducted in Ames medium.

In this report we take advantage of large-scale, high-density MEA recordings to quantify aspects of WT retinal wave activity patterns and determine how these patterns differ in the β2KO mouse. We find that a previously undetected directional bias, coupled with precisely correlated, high-frequency spiking, contributes to different aspects of refinement in the visual pathway of mice: fine-scale topography in the retinocollicular projection and eye-specific segregation in the retinogeniculate projection. Although the loss of the β2 gene and the defects in both retinal waves and refinement are only correlated, pharmacological perturbation of retinal waves affects refinement in vivo, supporting a causal link between wave dynamics and refinement of retinofugal projections (Stellwagen and Shatz, 2002; Cang et al., 2005; Pfeiffenberger et al., 2005). Thus, the ability to monitor the properties of a large number of neurons in the same preparation allowed us to identify critical features of patterned neural activity in the retina that are likely to be used by many aspects of CNS development and plasticity outside of the visual system.

NIH-PA Author Manuscript

NIH-PA Author Manuscript

NIH-PA Author Manuscript

Materials and Methods

Mice were maintained in the animal facility at the University of California at Santa Cruz (UCSC) and used in accordance with protocols approved by the UCSC Institutional Animal Care and Use Committee. Wild type mice were from the C57BL/6 strain. β2 mutations were genotyped as previously described (Xu et al., 1999).

MEA recording

After sacrificing, a hole was poked in the left eye with a needle to mark one pole of the retina. The eye was removed, and transferred to buffered Ames' medium (Sigma). The retina was dissected out and hemisected along either the nasal-temporal or dorsal-ventral axis, using the hole to orient the retina. The isolated retinal half was mounted on a piece of filter paper (Millipore SCWP01300) and placed RGC-side down onto a custom-built MEA that contained 512 electrodes arranged in 16 rows × 32 columns with 5 μm diameter electrodes and 60 μm spacing (Litke et al., 2004; Shlens et al., 2006; Petrusca et al., 2007; Elstrott et al., 2008). The piece of retina was held in place using a piece of coarse mesh strung across a metal ring. The recording chamber was superfused with Ames' solution at 3 ml/min containing Penicillin/Streptomycin bubbled with 95% O_2 and 5% O_2 and maintained at either 30°C or 37°C, pH 7.4. Each preparation was allowed to equilibrate for at least 30′ before data acquisition commenced.

Neuron identification

The voltage trace on each electrode was sampled at 20 kHz and stored for off-line analysis. Spikes that crossed a threshold of three times the root mean square noise on a seed electrode were sorted according to the principal components of their voltage waveforms on the seed electrode and its six nearest neighbors. Spikes were projected into the first five principal component dimensions, where an expectation maximization algorithm was used to sort spikes based on a mixture of Gaussians model (Litke et al., 2004).

To verify that each cluster came from a single cell, neuron candidates that lacked a refractory period in their autocorrelation function were considered contaminated by other neurons and excluded. Each candidate neuron was also inspected manually; the shape of the somatic waveform in its electrophysiological image was used to eliminate contaminated neuron candidates (Litke et al., 2004; Petrusca et al., 2007). Additionally, neurons whose mean spike rates were below one half of the mean spike rate of all neurons from a given preparation were excluded from further analysis. The mean spike rate was calculated by summing the total number of spikes and dividing by the length of the recording. This cut was performed to improve the reliability of the burst finding algorithm (see below) for neurons with low spike counts. To verify that our findings did not depend on the exclusion of these neurons, we performed the same analyses on all the neurons and obtained qualitatively similar results. After this cut, over 80% of all neurons from WT preparations and over 70% of all neurons from β2KO preparations were analyzed.

Wave analysis

To determine how frequently cells participated in waves, we defined wave occurrence quantitatively using a modified Poisson surprise algorithm (Legendy and Salcman, 1985; Demas et al., 2003). First the mean spike rate, λ, was computed for each single-unit spike train. Then, using a 1 s bin, the time-varying spike count, C, was computed for the spike train. The probability, P_{Ci}, that a Poisson spike train with mean spike rate λ would have C_i spikes in the ith time bin is:

NIH-PA Author Manuscript

NIH-PA Author Manuscript

NIH-PA Author Manuscript

$$P_{c_i} = e^{-(\lambda)} \times \frac{(\lambda)^{c_i}}{C_i!} \quad (1)$$

When the probability that a Poisson spike train would generate the spike count in a particular 1 s bin was $< 10^{-5}$, the cell under investigation was considered to be bursting. A wave was considered to have started when >5% of all the neurons identified in the recording were bursting. A wave was considered to have ended when <2.5% of all the neurons identified in a recording were still bursting. Waves detected using this algorithm were in excellent agreement with those selected by eye.

Burst analysis

To determine when RGCs fired bursts, we defined burst occurrence quantitatively using a modification of the wave analysis algorithm outlined above. First the mean inter-spike interval (ISI), ∂, was calculated for the neuron. The spike train for each neuron was then analyzed and, when at least three spikes were found such that their mean ISI $< \partial/2$, the algorithm checked for a possible burst. The initial probability, P_{Ci}, that a neuron with a mean spike rate, λ, would have C_i spikes in a time bin, T, where T is the time between the first and last spikes under investigation, was calculated as follows:

$$P_{c_i} = e^{-(\lambda \times T)} \times \frac{(\lambda \times T)^{c_i}}{C_i!} \quad (2)$$

Spikes were then added to the burst until either P_{Ci} including the new spike was greater than the initial value, or the next spike occurred more than ∂ after the preceding spike. A neuron was said to have fired a burst if the maximum P_{Ci} was less than 10^{-4}. The start of the burst was considered the time of the first spike and the end of the burst was considered the time of the last spike. This algorithm was sufficient for detecting bursts that were in agreement with those selected by eye.

Burst parameters

We computed several measures of spiking properties for each neuron. Burst durations, burst spike rates, and bursts ISIs were computed by averaging all values over the entire recording for each neuron. The time spent spiking above 10 Hz was computed by summing all ISIs < 100 ms within a burst. To quantify how high-frequency spiking was distributed amongst wave-bursts and non-wave-bursts, we calculated the percentage of the total time spent spiking above 10 Hz that occurred during wave-bursts or during non-wave-bursts. The correlation index (CI) was computed as described previously using a 100 msec coincidence interval (Wong et al., 1993). Because of the difference in spiking characteristics of β2KO RGCs, we calculated the CI using different portions of our datasets: 20 min, 1 hr, and the full recording. There was no affect on the differences between WT and β2KO CIs (Figure S5).

To assess the implications of the directional bias of waves, we calculated the offset correlation index (OCI) by grouping RGC pairs that fell within ±35° of the average angle of wave direction or the angle orthogonal to the average wave direction of a given preparation. For this calculation, we analyzed bursts that were offset in time by an amount, ΔO. The OCI was calculated using the following equation:

NIH-PA Author Manuscript

NIH-PA Author Manuscript

NIH-PA Author Manuscript

$$\mathrm{OCI}=\frac{[N_{AB(-\Delta O\pm 1.0s,+\Delta O\pm 1.0s)}\times T]}{[N_{A(0,T)}\times N_{B(0,T)}\times(2\times 1.0)]} \quad (4)$$

where $N_{AB}(-\Delta o\pm 0.5s, +\Delta o\pm 0.5s)$ is the number of bursts from cell B that fall within a 1 sec coincidence interval, ΔO seconds before, and ΔO seconds after, a burst from cell A, *T* is the duration of the recording in seconds, and $N_{A(0,\ T)}$ and $N_{B(0,\ T)}$ are the total number of bursts fired during waves from cell A and B during the recording. To calculate the OCI ratio as a function of intercellular distance, we divided the OCI value in the wave direction by the OCI value in the direction orthogonal to the wave direction at each bin.

To calculate the burst correlation index (BCI), all spikes that composed periods of spiking above 10 Hz were isolated from each burst. The median of these high-frequency spikes was used to calculate the BCI using the following formula:

$$\mathrm{BCI}=\frac{[B_{AB(-0.1s,+0.1s)}\times T]}{[B_{A(0,T)}\times B_{B(0,T)}\times 0.2s]} \quad (5)$$

where $B_{AB(-0.1s,\ +0.1s)}$ is the number of times the median of high-frequency spiking from cell B occurred within 100 ms of the median of the high-frequency spiking from cell A, *T* is the duration of the recording in seconds, and $B_{A(0,\ T)}$ and $B_{B(0,\ T)}$ are the total number of high-frequency bursts from cell A and B during the recording.

For all correlation calculations, mean values were calculated as follows: For each preparation, correlations were binned at 50 μm intervals and mean values calculated at each bin to create a correlation versus distance curve. These values were then averaged across preparations at each bin and plotted with standard errors to compare across genotypes. The resulting error is dominated by systematic (preparation-to-preparation variability) rather than by statistical effects.

Wave directionality analysis

To determine whether waves travel with a directional bias, we quantified how spontaneous activity traveled through individual neurons. To eliminate bias caused by the aspect ratio of our array, we only analyzed neurons detected in a central, square portion of the array containing 256 electrodes. For each neuron, we found all the bursts that occurred during waves (wave-bursts). For each wave-burst, we grouped all the neurons that were bursting within a 500 ms coincidence interval before (pre-bursting) and after (post-bursting) the wave-burst under investigation. To account for unusual wave topologies, we only included neurons that were up to 7 electrodes away (420 μm) from the electrode on which the neuron producing the wave-burst was detected. We calculated the center of mass (COM) of the pre- and post-bursting neurons as follows:

$$\mathrm{COM}=\frac{\sum_{i=1}^{n}(s_i\times r_i)}{\sum_{i=1}^{n}s_i} \quad (6)$$

NIH-PA Author Manuscript

NIH-PA Author Manuscript

NIH-PA Author Manuscript

where r_i is the location of a pre or post-bursting neuron and s_i is the number of spikes fired by neuron r during its burst. The angle, θ_b, between these two points was considered the direction of wave travel. Each spike in the wave-burst was represented as a vector with R=1 and $\theta = \theta_b$. We computed a normalized vector sum of all the spike vectors from all the wave-bursts from a given neuron to generate the neuron directional bias vector (nDB). A neuron had a significant directional bias if the distribution of spike angles deviated significantly from circular uniformity (Rayleigh Test; $p < 0.05$). To determine whether a given preparation had a direction preference, we calculated the preparation directional bias vector (pDB) which is the normalized vector sum of all of the nDBs. A preparation had a significant directional bias if the distribution of nDBs deviated significantly from circular uniformity (Rayleigh Test; $p < 0.01$).

Wavefront width

To estimate the width of the wave-front, we identified neurons that burst during a wave as outlined above. The width was defined as the maximum distance between any pair of neurons in the group or pre and post-bursting neurons. The width of the wave-front for a given wave was the mean of all these calculations for all the bursts that composed the wave.

Wave Speed

To estimate wave speed we isolated spikes from neurons that took place during waves. We then binned each wave into one second intervals and calculated the center of mass of all the neurons that fired spikes during each bin weighted by the number of spikes they fired during the bin (6). The distance between consecutive centers of mass was used to calculate an instantaneous wave speed for each bin. The total speed of the wave was the average of all the instantaneous speeds.

Supplementary Material

Refer to Web version on PubMed Central for supplementary material.

Acknowledgments

We thank M. Feller, A. D. Huberman, and J. Yamada for discussions and critical reading of the manuscript. We gratefully acknowledge the technical contributions of W. Dabrowski, A. Grillo, M. Grivich, P. Grybos, P. Hottowy, S. Kachiguine and D. Petrusca. This work was supported by a US National Institutes of Health (NIH) grant EYO14689 (D.A.F), a QB3 Seed Grant (D.A.F.), a National Science Foundation grant PHY-0750525 (A.M.L.), a Burroughs Wellcome Career Award at Scientific Interface (A.S.), and a UC Santa Cruz Chancellor's Fellowship (B.K.S.).

References

Bansal A, Singer JH, Hwang BJ, Xu W, Beaudet A, Feller MB. Mice lacking specific nicotinic acetylcholine receptor subunits exhibit dramatically altered spontaneous activity patterns and reveal a limited role for retinal waves in forming ON and OFF circuits in the inner retina. J Neurosci 2000;20:7672–681. [PubMed: 11027228]

Bjartmar L, Huberman AD, Ullian EM, Renteria RC, Liu X, Xu W, Prezioso J, Susman MW, Stellwagen D, et al. Neuronal pentraxins mediate synaptic refinement in the developing visual system. J Neurosci 2006;26:6269–281. [PubMed: 16763034]

Butts DA, Rokhsar DS. The information content of spontaneous retinal waves. J Neurosci 2001;21:961–973. [PubMed: 11157082]

Butts DA, Kanold PO, Shatz CJ. A burst-based “Hebbian” learning rule at retinogeniculate synapses links retinal waves to activity-dependent refinement. PLoS Biol 2007;5:e61. [PubMed: 17341130]

Cang J, Renteria RC, Kaneko M, Liu X, Copenhagen DR, Stryker MP. Development of precise maps in visual cortex requires patterned spontaneous activity in the retina. Neuron 2005;48:797–809. [PubMed: 16337917]

NIH-PA Author Manuscript

NIH-PA Author Manuscript

NIH-PA Author Manuscript

Chalupa LM. A reassessment of the role of activity in the formation of eye-specific retinogeniculate projections. Brain Res Rev 2007;55:228–236. [PubMed: 17433447]

Champagne FA, Curley JP, Keverne EB, Bateson PP. Natural variations in postpartum maternal care in inbred and outbred mice. Physiol Behav 2007;91:325–334. [PubMed: 17477940]

Chandrasekaran AR, Plas DT, Gonzalez E, Crair MC. Evidence for an instructive role of retinal activity in retinotopic map refinement in the superior colliculus of the mouse. J Neurosci 2005;25:6929–938. [PubMed: 16033903]

Chandrasekaran AR, Shah RD, Crair MC. Developmental homeostasis of mouse retinocollicular synapses. J Neurosci 2007;27:1746–755. [PubMed: 17301182]

Chen C, Regehr WG. Developmental remodeling of the retinogeniculate synapse. Neuron 2000;28:955–966. [PubMed: 11163279]

Chen YH, DeHaan RL. Temperature dependence of embryonic cardiac gap junction conductance and channel kinetics. J Membr Biol 1993;136:125–134. [PubMed: 7508979]

Dan Y, Poo MM. Spike timing-dependent plasticity: from synapse to perception. Physiol Rev 2006;86:1033–048. [PubMed: 16816145]

Demas J, Eglen SJ, Wong RO. Developmental loss of synchronous spontaneous activity in the mouse retina is independent of visual experience. J Neurosci 2003;23:2851–860. [PubMed: 12684472]

Demas J, Sagdullaev BT, Green E, Jaubert-Miazza L, McCall MA, Gregg RG, Wong RO, Guido W. Failure to maintain eye-specific segregation in nob, a mutant with abnormally patterned retinal activity. Neuron 2006;50:247–259. [PubMed: 16630836]

Elstrott J, Anishchenko A, Greschner M, Sher A, Litke AM, Chichilnisky EJ, Feller MB. Direction selectivity in the retina is established independent of visual experience and cholinergic retinal waves. Neuron 2008;58:499–506. [PubMed: 18498732]

Feller MB, Butts DA, Aaron HL, Rokhsar DS, Shatz CJ. Dynamic processes shape spatiotemporal properties of retinal waves. Neuron 1997;19:293–306. [PubMed: 9292720]

Feller MB, Wellis DP, Stellwagen D, Werblin FS, Shatz CJ. Requirement for cholinergic synaptic transmission in the propagation of spontaneous retinal waves. Science 1996;272:1182–87. [PubMed: 8638165]

Godement P, Salaun J, Imbert M. Prenatal and postnatal development of retinogeniculate and retinocollicular projections in the mouse. J Comp Neurol 1984;230:552–575. [PubMed: 6520251]

Grubb MS, Rossi FM, Changeux JP, Thompson ID. Abnormal functional organization in the dorsal lateral geniculate nucleus of mice lacking the beta 2 subunit of the nicotinic acetylcholine receptor. Neuron 2003;40:1161–172. [PubMed: 14687550]

Huberman AD. Mechanisms of eye-specific visual circuit development. Curr Opin Neurobiol 2007;17:73–80. [PubMed: 17254766]

Huberman AD, Feller MB, Chapman B. Mechanisms underlying development of visual maps and receptive fields. Annu Rev Neurosci 2008;31:479–509. [PubMed: 18558864]

Katz LC, Shatz CJ. Synaptic activity and the construction of cortical circuits. Science 1996;274:1133–38. [PubMed: 8895456]

Legendy CR, Salcman M. Bursts and recurrences of bursts in the spike trains of spontaneously active striate cortex neurons. J Neurophysiol 1985;53:926–939. [PubMed: 3998798]

Litke AM, Bezayiff N, Chichilnisky EJ, Cunningham W, Dabrowski W, Grillo AA, Grivich MI, Grybos P, Hottowy P, et al. What does the eye tell the brain?: Development of a system for the large-scale recording of retinal output activity. IEEE Transactions on Nuclear Science 2004;51:1434–440.

McLaughlin T, Torborg CL, Feller MB, O'Leary DD. Retinotopic map refinement requires spontaneous retinal waves during a brief critical period of development. Neuron 2003;40:1147–160. [PubMed: 14687549]

Meister M, Wong RO, Baylor DA, Shatz CJ. Synchronous bursts of action potentials in ganglion cells of the developing mammalian retina. Science 1991;252:939–943. [PubMed: 2035024]

Mrsic-Flogel TD, Hofer SB, Creutzfeldt C, Cloëz-Tayarani I, Changeux JP, Bonhoeffer T, Hübener M. Altered map of visual space in the superior colliculus of mice lacking early retinal waves. J Neurosci 2005;25:6921–28. [PubMed: 16033902]

NIH-PA Author Manuscript

NIH-PA Author Manuscript

NIH-PA Author Manuscript

Muir-Robinson G, Hwang BJ, Feller MB. Retinogeniculate axons undergo eye-specific segregation in the absence of eye-specific layers. J Neurosci 2002;22:5259–264. [PubMed: 12097474]

Pauluhn J, Schmuck G. Critical analysis of potential body temperature confounders on neurochemical endpoints caused by direct dosing and maternal separation in neonatal mice: a study of bioallethrin and deltamethrin interactions with temperature on brain muscarinic receptors. J Appl Toxicol 2003;23:9–18. [PubMed: 12518331]

Penn AA, Riquelme PA, Feller MB, Shatz CJ. Competition in retinogeniculate patterning driven by spontaneous activity. Science 1998;279:2108–112. [PubMed: 9516112]

Petrusca D, Grivich MI, Sher A, Field GD, Gauthier JL, Greschner M, Shlens J, Chichilnisky EJ, Litke AM. Identification and characterization of a Y-like primate retinal ganglion cell type. J Neurosci 2007;27:11019–027. [PubMed: 17928443]

Pfeiffenberger C, Cutforth T, Woods G, Yamada J, Renteria RC, Copenhagen DR, Flanagan JG, Feldheim DA. Ephrin-As and neural activity are required for eye-specific patterning during retinogeniculate mapping. Nat Neurosci 2005;8:1022–27. [PubMed: 16025107]

Picciotto MR, Zoli M, Léna C, Bessis A, Lallemand Y, Le Novère N, Vincent P, Pich EM, Brûlet P, Changeux JP. Abnormal avoidance learning in mice lacking functional high-affinity nicotine receptor in the brain. Nature 1995;374:65–67. [PubMed: 7870173]

Plas DT, Lopez JE, Crair MC. Pretarget sorting of retinocollicular axons in the mouse. J Comp Neurol 2005;491:305–319. [PubMed: 16175549]

Remtulla S, Hallett PE. A schematic eye for the mouse, and comparisons with the rat. Vision Res 1985;25:21–31. [PubMed: 3984214]

Schmucker C, Schaeffel F. A paraxial schematic eye model for the growing C57BL/6 mouse. Vision Res 2004;44:1857–867. [PubMed: 15145680]

Shatz CJ, Stryker MP. Prenatal tetrodotoxin infusion blocks segregation of retinogeniculate afferents. Science 1988;242:87–89. [PubMed: 3175636]

Shlens J, Field GD, Gauthier JL, Grivich MI, Petrusca D, Sher A, Litke AM, Chichilnisky EJ. The structure of multi-neuron firing patterns in primate retina. J Neurosci 2006;26:8254–266. [PubMed: 16899720]

Simon DK, O'Leary DDM. Development of topographic order in the mammalian retinocollicular projection. J Neurosci 1992;12:1212–232. [PubMed: 1313491]

Singer JH, Mirotznik RR, Feller MB. Potentiation of L-type calcium channels reveals nonsynaptic mechanisms that correlate spontaneous activity in the developing mammalian retina. J Neurosci 2001;21:8514–522. [PubMed: 11606640]

Sjöström PJ, Turrigiano GG, Nelson SB. Rate, timing, and cooperativity jointly determine cortical synaptic plasticity. Neuron 2001;32:1149–164. [PubMed: 11754844]

So KF, Campbell G, Lieberman AR. Development of the mammalian retinogeniculate pathway: target finding, transient synapses and binocular segregation. J Exp Biol 1990;153:85–104. [PubMed: 2280230]

Stacy RC, Demas J, Burgess RW, Sanes JR, Wong RO. Disruption and recovery of patterned retinal activity in the absence of acetylcholine. J Neurosci 2005;25:9347–357. [PubMed: 16221843]

Stellwagen D, Shatz CJ. An instructive role for retinal waves in the development of retinogeniculate connectivity. Neuron 2002;33:357–367. [PubMed: 11832224]

Sun C, Speer CM, Wang G, Chapman B, Chalupa LM. Epibatidine application in vitro blocks retinal waves without silencing all retinal ganglion cell action potentials in developing retina of the mouse and ferret. J Neurophysiol. 2008

Sun C, Warland DK, Ballesteros JM, van der List D, Chalupa LM. Retinal waves in mice lacking the beta2 subunit of the nicotinic acetylcholine receptor. Proc Natl Acad Sci U S A 2008;105:13638–643. [PubMed: 18757739]

Torborg CL, Feller MB. Spontaneous patterned retinal activity and the refinement of retinal projections. Prog Neurobiol 2005;76:213–235. [PubMed: 16280194]

Torborg CL, Hansen KA, Feller MB. High frequency, synchronized bursting drives eye-specific segregation of retinogeniculate projections. Nat Neurosci 2005;8:72–78. [PubMed: 15608630]

Usrey WM, Reppas JB, Reid RC. Paired-spike interactions and synaptic efficacy of retinal inputs to the thalamus. Nature 1998;395:384–87. [PubMed: 9759728]

NIH-PA Author Manuscript

NIH-PA Author Manuscript

NIH-PA Author Manuscript

Valiunas V, Manthey D, Vogel R, Willecke K, Weingart R. Biophysical properties of mouse connexin30 gap junction channels studied in transfected human HeLa cells. J Physiol 1999;519(Pt 3):631–644. [PubMed: 10457079]

Wong ROL, Meister M, Shatz CJ. Transient period of correlated bursting activity during development of the mammalian retina. Neuron 1993;11:923–938. [PubMed: 8240814]

Xu W, Orr-Urtreger A, Nigro F, Gelber S, Sutcliffe CB, Armstrong D, Patrick JW, Role LW, Beaudet AL, De Biasi M. Multiorgan autonomic dysfunction in mice lacking the beta2 and the beta4 subunits of neuronal nicotinic acetylcholine receptors. J Neurosci 1999;19:9298–9305. [PubMed: 10531434]

NIH-PA Author Manuscript
NIH-PA Author Manuscript
NIH-PA Author Manuscript

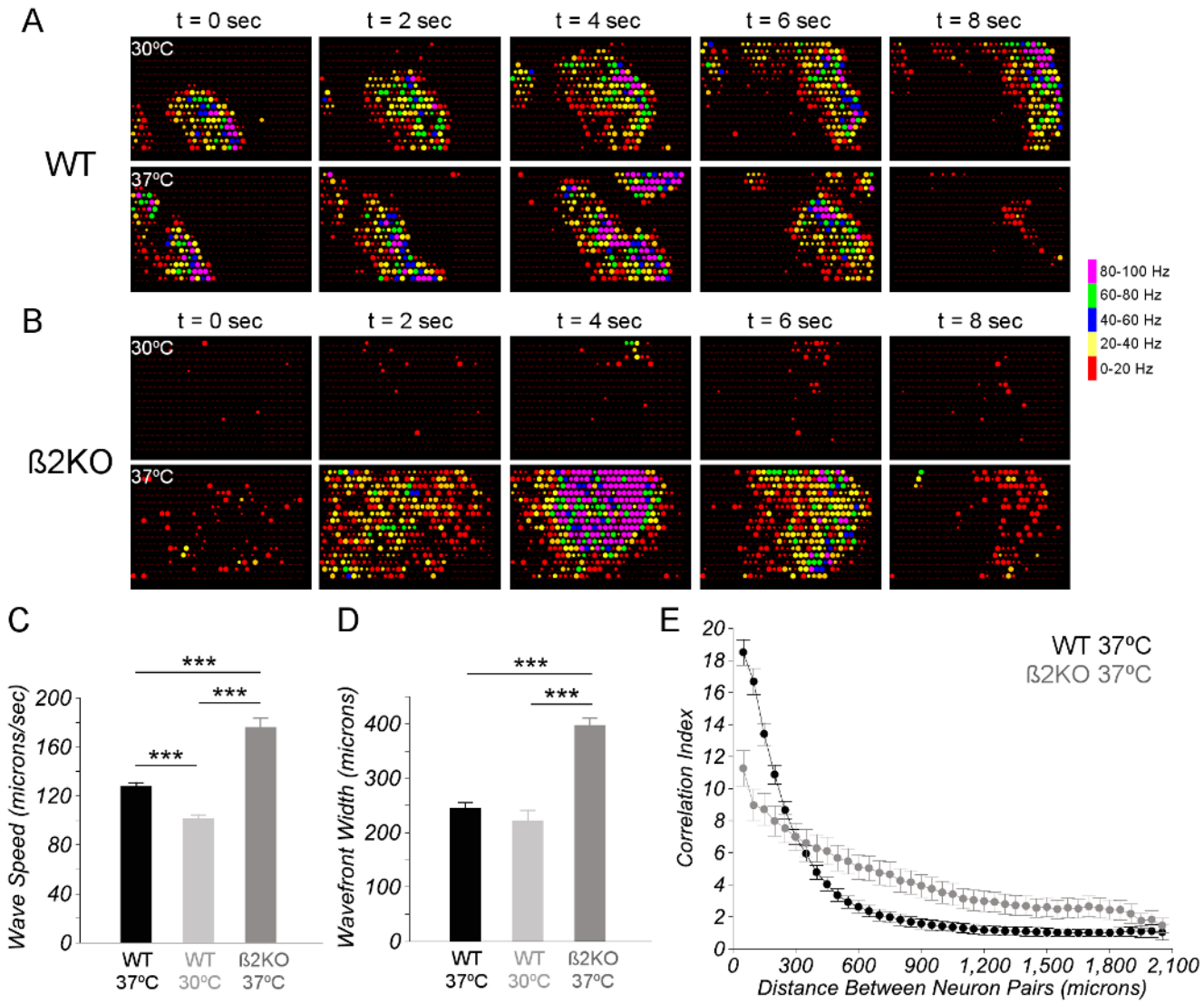

Figure 1.

MEA recordings of spontaneous activity reveal that retinal waves are present at 37°C but not 30°C in β2KO. (**A**) Examples of waves recorded from the same P6 WT retina at 30°C (top) and 37°C (bottom). (**B**) Examples of waves recorded from the same P6 β2KO retina at 30°C (top) and 37°C (bottom). Each dot represents multiunit activity recorded on an electrode at that site. The size of the dot is proportional to the amplitude of the spikes detected on the electrode and the color represents their frequency. Electrode spacing is 60 μm. (**C**) In WT retinas, waves travel faster at 37°C (black) than they do at 30°C (light gray) while, in β2KO retinas at 37°C (gray), waves travel even faster than in WT retinas at either temperature ($p < 0.0001$; one-way ANOVA with Bonferroni adjustment). (**D**) Quantification of the width of the wave front demonstrates that at 37°C, β2KO (gray) wave fronts are wider than WT wave fronts at either 30°C (light gray) or 37°C (black; $p < 0.0001$; one-way ANOVA with Bonferroni adjustment). Data in (C) and (D) are from WT 37°C: 2993 waves from 17 retinas; WT 30°C: 607 waves from 7 retinas; β2KO 37°C: 750 waves from 12 retinas. (**E**) Correlation index computed for spike trains from pairs of neurons and plotted as a function of the distance between electrodes on which the neurons were recorded. Plot summarizes data from multiple WT (black; n = 17)

and β2KO (gray; n = 12) preparations and shows that CI decreases as a function of distance in both WT and β2KO retina. Error bars represent SEM. *** $p < 0.001$.

NIH-PA Author Manuscript
NIH-PA Author Manuscript
NIH-PA Author Manuscript

NIH-PA Author Manuscript
NIH-PA Author Manuscript
NIH-PA Author Manuscript

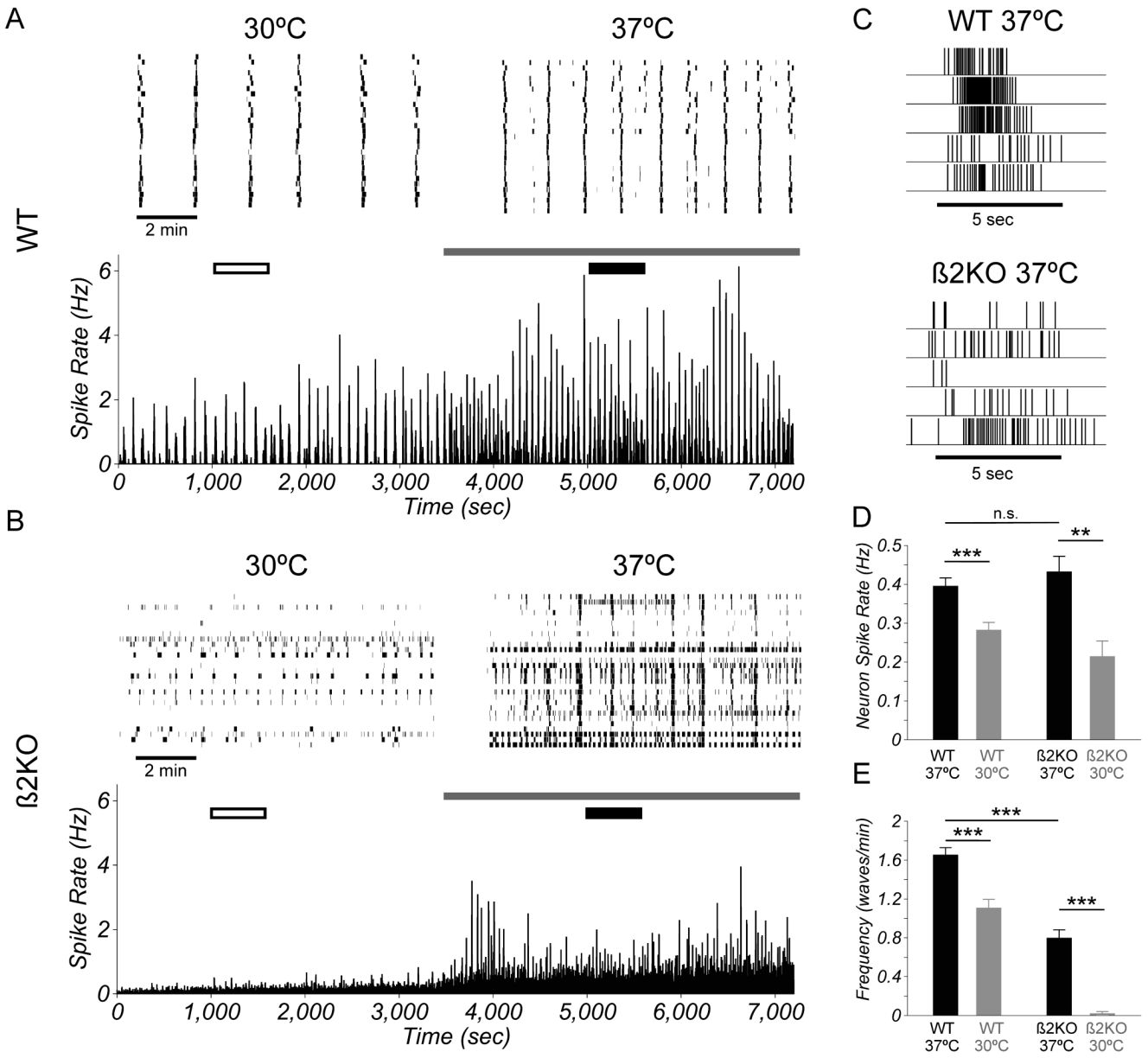

Figure 2.

Temperature induces changes in spontaneous activity patterns of RGCs in WT and β2KO. (**A**) Peristimulus time histograms (PSTHs) of the mean spike rate of all neurons (bottom) at 30°C and 37°C (denoted by gray bar) from a P6 WT retina as well as single unit activity of 30 RGCs from a ten minute segment of the recording at 30°C (top left; denoted by open bar in bottom) and 37°C (top right; denoted by black bar in bottom). (**B**) PSTHs of the mean spike rate of all neurons (bottom) at 30°C and 37°C (denoted by gray bar) from a P6 β2KO retina as well as single unit activity of 30 RGCs from a ten min segment of the recording at 30°C (top left; denoted by open bar in bottom) and 37°C (top right; denoted by black bar in bottom). Correlated activity is seen at 37°C but not 30°C in the β2KO and the pattern of this activity is considerably different from WT patterns at either 30°C or 37°C. (**C**) High resolution spike rasters from WT (top) and β2KO (bottom) demonstrate that β2KO bursts appear to contain fewer spikes than WT. (**D**) RGCs spike more at 37°C (black) than at 30°C (gray) in both WT

(left) and β2KO (right) retinas. (**E**) Waves occur more frequently at 37°C (black) than at 30° C (gray) in both WT (left) and β2KO (right) retinas. Data in (D) and (E) are from WT 37°C: 4378 neurons from 17 retinas; WT 30°C: 1331 neurons from 7 retinas, β2KO 37°C: 4078 neurons from 12 retinas, and β2KO 30°C: 2127 neurons from 6 retinas. Error bars represent SEM. ** $p < 0.01$; *** $p < 0.001$.

NIH-PA Author Manuscript
NIH-PA Author Manuscript
NIH-PA Author Manuscript

NIH-PA Author Manuscript

NIH-PA Author Manuscript

NIH-PA Author Manuscript

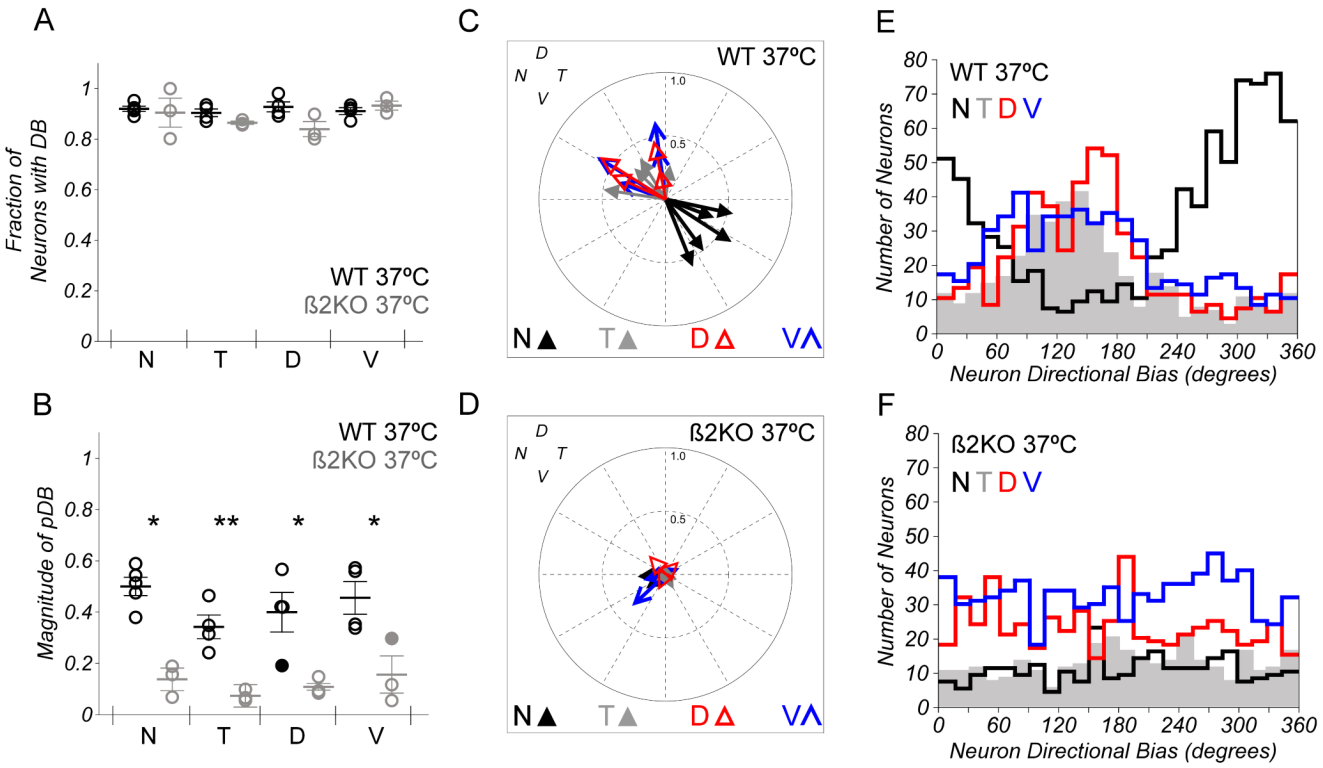

Figure 3.

Retinal waves travel in a preferred direction in WT but not β2KO retina. (**A**) A comparison of the fraction of neurons in each preparation that display a directional bias indicates that WT (black) and β2KO (gray) retinas have equivalent amounts of RGCs that display a directional bias (see Methods; p = 0.1522, Kruskal-Wallis ANOVA; WT: 2354 neurons from 17 retinas; β2KO: 1888 neurons from 12 retinas). (**B**) A comparison of the magnitude of the preparation directional bias demonstrates that β2KO retinas (gray) have less directional bias than WT (black). A large preparation directional bias indicates that waves possess a directional bias in a given recording (Nasal to Nasal: p = 0.01772; Temporal to Temporal: p = 0.00768; Dorsal to Dorsal: p = 0.0292; Ventral to Ventral: p = 0.02933; t-tests). Black filled circle indicates a WT preparation lacking a directional bias and a gray filled circle indicates a β2KO preparation with a directional bias. (**C, D**) Polar plots measuring the preparation directional bias of individual preparations from nasal (black), temporal (light gray), dorsal (dark gray; open arrowheads), and ventral (gray; arrow points) retinas. Each arrow represents the mean direction (angle) and mean strength (magnitude) of the directional bias of all the RGCs in an individual preparation and shows that retinal waves have a preferred direction in WT but not β2KO retinas. (C) WT preparations from each retinal quadrant have a directional bias (see Table 2) and the angle of bias is the same in Dorsal, Ventral, and Temporal retina, but of opposite polarity in Nasal retina ($p < 0.05$; Circular ANOVA with Wheeler-Watson test with Bonferroni correction). (D) β2KO preparations lack a directional bias (see Table 2) and the angle is the same in all quadrants in β2KO retina (p = 0.289; Circular ANOVA). (**E, F**) Distributions of angle of neuron directional bias for individual RGCs indicate that WT preparations (E) possess a directional bias in each quadrant while β2KO preparations (F) do not (Nasal: black, Temporal: filled, light gray, Dorsal: dark gray, Ventral: gray). In (A) and (B), plot shows values (circles) along with means (horizontal lines) and SEMs. N: Nasal; T: Temporal; D: Dorsal; V: Ventral; ** $p < 0.01$; * $p < 0.05$.

NIH-PA Author Manuscript

NIH-PA Author Manuscript

NIH-PA Author Manuscript

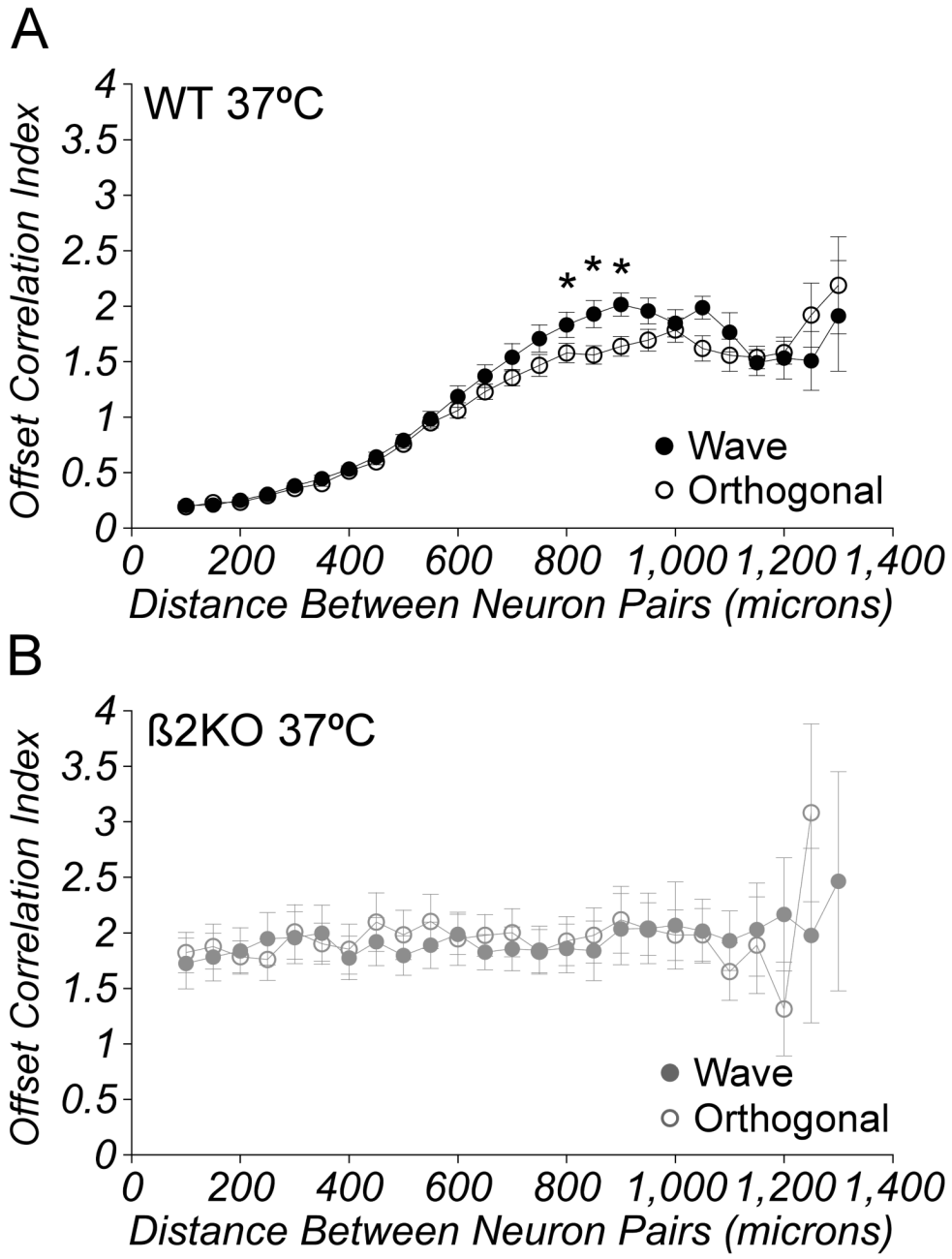

Figure 4.

The probability that spatially distant RGCs will fire temporally-offset bursts is increased in an axis-specific manner in WT, but not β2KO retinas. Offset Correlation Indices (OCIs) computed for bursts fired during waves from pairs of neurons and plotted as a function of the distance between electrodes on which the neurons were recorded. (**A**) OCIs are larger for WT RGCs separated by 800-900 μm along the NT axis (filled circles) than along the axis orthogonal to it for time offsets of 4-5 seconds (open circles; 17 retinas; 209,566 RGC pairs) (**B**) In β2KOs retinas, OCIs are equivalent along both axes at the same time offset as in (A) (12 retinas; 257,567 RGC pairs). Error bars represent SEM. * $p < 0.05$.

NIH-PA Author Manuscript
NIH-PA Author Manuscript
NIH-PA Author Manuscript

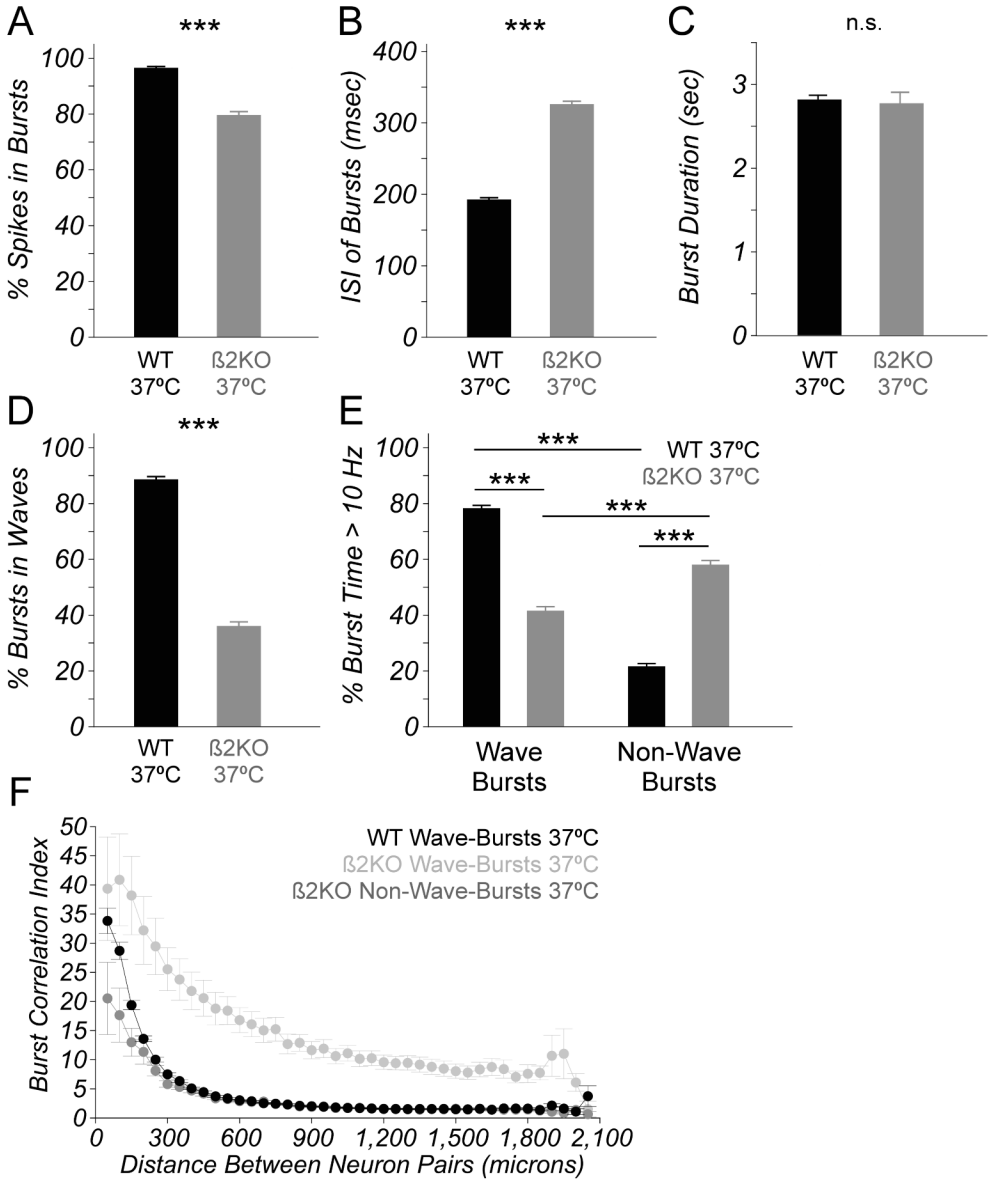

Figure 5.

β2KO RGCs fire bursts that contain fewer spikes and are less correlated than those in WT retina. (**A**) The percent of all spikes that are included in bursts is significantly reduced in β2KO RGCs (gray). (**B**) Inter-spike intervals (ISI) of bursts are significantly increased in β2KO RGCs (gray). (**C**) The mean burst duration is unchanged in β2KOs (gray). (**D**) A comparison of the percentage of all bursts that occur during waves reveals that the bulk of RGC bursts occur during waves in WT retinas (black), but in between waves in β2KO retinas (gray; WT: 2993 waves; β2KO: 760 waves; same number of bursts as A and B). (**E**) The bulk of high-frequency spiking occurs during wave-bursts in WT RGCs (left, black), but during non-wave-bursts in β2KO RGCs (right, gray). Data in (A-E) are from WT: 234,154 bursts from 4378 RGCs; β2KO: 369,124 bursts from 4078 RGCs. (**F**) Burst correlation index computed for bursts from pairs of neurons and plotted as a function of the distance between electrodes on which the neurons were recorded. Plot summarizes data from multiple WT (209,566 RGC wave pairs) and β2KO (430,088 RGC wave pairs and 257,567 RGC non-wave pairs) preparations and

shows that BCI decreases as a function of distance for wave-bursts from WT (black) and β2KO (light gray) retina, but is significantly reduced in non-wave-bursts (gray) from β2KO retina. Data in (A-E) are from WT: 17 retinas, β2KO: 12 retinas. Error bars represent SEM. *** $p < 0.001$. n.s. not significant.

NIH-PA Author Manuscript
NIH-PA Author Manuscript
NIH-PA Author Manuscript

NIH-PA Author Manuscript

NIH-PA Author Manuscript

NIH-PA Author Manuscript

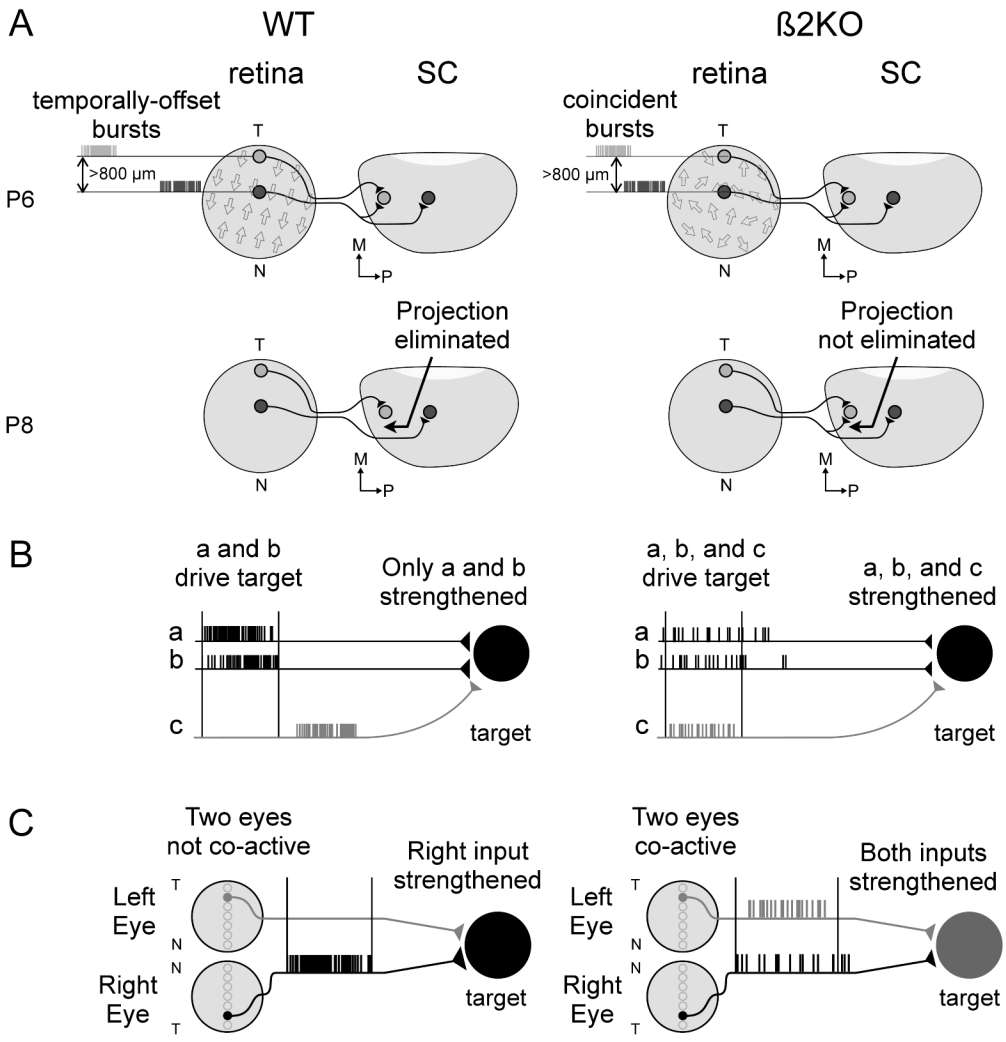

Figure 6.

Models of how retinal waves mediate the refinement of visual system projections. (**A**) Synapse elimination: In WT mice, the directional bias of retinal waves along the NT axis during the first post-natal week helps refine projections along this axis by ensuring that RGCs separated by 800+ µm are more likely to fire temporally-offset bursts (top left, wave direction designated by arrows in retina; see Figure 4). This helps eliminate topographically incorrect projections by the second week (bottom left). Because the directional bias of waves is lost in β2KOs, this decreases the likelihood that RGCs separated by 800+ µm will fire temporally-offset bursts (top right). Topographically incorrect synapses are not eliminated and axonal projections fail to refine along the NT axis (bottom right). (**B**) Synapse strengthening: In WT retinal waves, short ISIs and strong local correlations within each eye ensure that only neighboring RGCs (a and b) drive post-synaptic bursting in target neurons, stabilizing these synapses but not ones from distant RGCs (c, left). In β2KOs, longer correlations allow distant RGCs (a,b, and c) to drive coincident post-synaptic spiking, stabilizing misdirected axonal projections (right). (**C**) Eye-specific segregation: In WT retinas, the lack of RGC activity during inter-wave intervals ensures that retinotopically matched regions of the two eyes are not co-active. This helps strengthen projections from one eye, thereby segregating inputs from the same eye (left). In

β2KOs, inter-wave activity is increased leading to an increased probability of co-active inputs. This strengthens inputs from both eyes and segregation fails to occur normally (right).

NIH-PA Author Manuscript
NIH-PA Author Manuscript
NIH-PA Author Manuscript

NIH-PA Author Manuscript

NIH-PA Author Manuscript

NIH-PA Author Manuscript

Table 1
Differences in the Discharge Properties of WT and β2KO RGCs

Means ± standard deviations are reported for measurements of RGC spiking properties. Significance for comparisons between WT and β2KO recordings for each spiking property is indicated by asterisks (T-test). * $p < 0.05$; ** $p < 0.01$; *** $p < 0.001$.

All Neurons	**P6 WT 37°C**	**P6 β2KO 37°C**
Neurons	258 ± 99	340 ± 161
Neuron Spike Rate (spikes/sec)	0.396 ± 0.087	0.433 ± 0.136
Wave Frequency (waves/min)	1.66 ± 0.30	0.80 ± 0.28 ***
Wave Duration (sec)	13.0 ± 2.8	10.8 ± 3.3
All Bursts		
Burst Frequency (bursts/min)	1.0 ± 0.1	2.1 ± 0.7 ***
Burst ISI (msec)	192.7 ± 28.7	326.2 ± 59.9 ***
% Spikes in Bursts	96.6 ± 1.0	79.6 ± 5.1 ***
% Total Burst Time > 10 Hz	23.2 ± 6.5	11.5 ± 1.9 ***
% Bursts in Waves	88.7 ± 3.6	36.1 ± 7.4 ***
Wave Bursts		
Burst Duration (sec)	2.96 ± 0.25	3.18 ± 0.57
Burst ISI (msec)	189.2 ± 27.4	302.9 ± 55.5 ***
% Burst Time > 10 Hz	78.3 ± 4.2	41.6 ± 7.2 ***
Bursts/Neuron/Wave:	1.02 ± 0.02	1.18 ± 0.12 **
Non Wave Bursts		
Burst Duration (sec)	2.68 ± 0.18	2.38 ± 0.40 *
Burst ISI (msec)	204.4 ± 33.1	338.1 ± 66.1 ***
% Burst Time > 10 Hz	21.7 ± 4.2	58.1 ± 7.2 ***

NIH-PA Author Manuscript

NIH-PA Author Manuscript

NIH-PA Author Manuscript

Table 2

Summary of Directional Bias

Circular means ± circular variance are reported for measurements of the angle of directional bias from each retinal pole. Significance for the determination of whether the angles of directional bias from multiple preparations from a retinal pole deviated significantly from circular uniformity is indicated by asterisks (Rayleigh test). The number of retinas analyzed are given for each retinal pole. * $p < 0.05$; ** $p < 0.01$.

P6 WT Mean Angle	
Retinal Pole	**Angle (deg)**
Nasal (n = 5)	322.69 ± 3.68 **
Temporal (n = 4)	127.88 ± 8.38 *
Dorsal (n = 4)	126.53 ± 5.54 *
Ventral (n = 4)	126.12 ± 14.22 *
P6 β2KO Mean Angle	
Retinal Pole	**Angle (deg)**
Nasal (n = 3)	218.45 ± 7.20
Temporal (n = 3)	287.39 ± 21.07
Dorsal (n = 3)	124.48 ± 45.02
Ventral (n = 3)	214.49 ± 39.23